Howard Hughes Medical Institute

Published as: *Nat Methods*. ; 8(7): 599–605.

High-content behavioral analysis of *Caenorhabditis elegans* in precise spatiotemporal chemical environments

Dirk R Albrecht and **Cornelia I Bargmann**
Howard Hughes Medical Institute and Laboratory of Neural Circuits and Behavior, The Rockefeller University, New York NY 10065

Abstract

To gain a quantitative understanding of chemosensory behaviors, it is desirable to present many animals with repeatable, well-defined chemical stimuli. To that end, we describe a microfluidic system to analyze *Caenorhabditis elegans* behavior in defined temporal and spatial stimulus patterns. A 2 × 2 cm^2 structured arena allowed *C. elegans* to perform crawling locomotion in a controlled liquid environment. We characterized behavioral responses to attractive odors with three stimulus patterns: temporal pulses, spatial stripes, and a linear concentration gradient, all delivered in the fluid phase to eliminate variability associated with air-fluid transitions. Different stimulus configurations preferentially revealed turning dynamics in a biased random walk, directed orientation into an odor stripe, and speed regulation by odor. We identified both expected and unexpected responses in wild-type animals and sensory mutants by quantifying dozens of behavioral parameters. The devices are inexpensive, easy to fabricate, reusable, and suitable for delivering any liquid-borne stimulus.

Introduction

The transformation of sensory information into behavioral output by a neural circuit can be examined with a systems identification procedure: probing the system, observing its response, and inferring its dynamics[1]. This quantitative approach depends on precise stimulus delivery to multiple animals and accurate measurements of response[2]. The nematode *Caenorhabditis elegans* is an ideal model for studying the interplay among genes, neurons, circuits and behavior, but it has been difficult to control and quantify chemical stimulus patterns presented to freely-behaving worms. The earliest examinations of *C. elegans* chemosensory behavior used point sources of concentrated stimuli to generate broad spatial gradients by chemical diffusion through agar or air[3,4], but these gradients were variable and changeable over time. Methods were then developed to present sudden step changes in gaseous or aqueous stimuli[5–7], but these assays had limited control of the exact

Correspondence should be addressed to D.R.A. (dirk.albrecht@gmail.com).

AUTHOR CONTRIBUTIONS

D.R.A. designed and fabricated the devices; D.R.A. wrote the analysis code; D.R.A. and C.I.B. designed the experiments; D.R.A. performed the experiments; D.R.A. analyzed the data; D.R.A. and C.I.B. wrote the paper.

chemical input at the sensory apparatus, especially for volatile odors that partition between air and liquid phases.

Closed microfluidic circuits simultaneously limit the influence of the external environment and enable precise, predictable spatial and temporal stimulus patterns when operated under laminar flow. Mammalian cells and unicellular organisms have been subjected to these dynamic chemical environments[8–10], and *C. elegans*, ~60 μm in diameter and 1 mm long, is also appropriately sized for microfluidic devices. In several recent applications for neuronal imaging, high-throughput phenotypic screens, and laser axotomy (reviewed in [11,12]), *C. elegans* could be completely immobilized, spatially restricted while permitting body posture movements[13], or allowed to navigate through undulating channels[14] or structured environments[14,15].

In this paper, we report a series of microstructured arenas optimized for normal *C. elegans* crawling behaviors and for well-controlled pulses, stripes, and linear spatial gradients of chemical stimuli. We quantify these spatiotemporal stimulus patterns and use automated behavioral classification software to analyze wild-type and mutant worms in various olfactory environments. We find that olfactory behaviors can be dissected into known and novel locomotory components, and identify genetic requirements for specific components of the olfactory response.

RESULTS

System design and overview

Behavioral arenas were composed of poly(dimethylsiloxane), a biologically-inert silicone, reversibly sealed to a hydrophobic glass substrate. Microfluidic designs featured: (1) a structured micropost array through which *C. elegans* moved; (2) upstream and downstream barriers that restricted animals to the arena; (3) stimulus inlets and an outlet; and (4) a worm loading port (Fig. 1a and Supplementary Notes). We optimized the arena geometry such that young adult hermaphrodites crawled with a sinusoidal motion at a similar speed, wavelength, and amplitude as they do on an agar plate (Supplementary Notes). Worms moved smoothly around hexagonally-arranged microposts, 200 μm in diameter and spaced 300 μm apart and were not compressed in the 70 μm deep arena (Fig. 1b and Supplementary Video 1).

Animals were in an entirely fluid-filled, well-oxygenated environment and exposed to liquid-borne stimuli that flowed by gravity from elevated reservoirs through manual or computer-actuated valves (Fig. 1c) and entered the arena through assay-specific inlet channels. For temporal pulses, inlets converged to a single channel and diverged through a distribution network (Fig. 1d), thereby generating a fluid interface perpendicular to the flow direction that swept across the arena and switched within 3 s (at a typical 1 mm s^{-1} velocity and minimally 0.3 s, Supplementary Figs. 1,2). For the stripe pattern, each inlet controlled a separate channel into the arena, resulting in stepwise variation of concentration perpendicular to flow (Fig. 1e) and a gradient width of 50–350 μm (Supplementary Figs. 1,3). Broad linear or sigmoidal spatial gradients were created with an upstream mixing tree of interconnected diverging channels (Fig. 1f and Supplementary Fig. 4). In all

configurations, stimulus gradients were highly stable for hours, repeatable across trials, experiments and devices, and dynamically tunable by fluid flowrate V (varying by $V^{1/2}$ for pulse and stripe assays and linearly for broad gradients, Supplementary Figs. 1–4).

Worm locomotion in behavioral arenas

On an agar surface, *C. elegans* moves forward with sinusoidal movement by head-to-tail propagation of dorsal and ventral body bends. Forward locomotion is interrupted by pauses, reversals, and "omega turns," in which the animal bends head to tail with a sharp change in direction[16]; a bout of one or more coupled reversals and omega turns is designated a "pirouette"[17]. *C. elegans* may also "curve," gradually reorienting during forward motion. In the microfluidic arena, worms performed all of these behaviors (Fig. 2a, Supplementary Video 1). We developed automated tracking software to identify five primary behavioral states: Forward (straight or curve), Pause, Reverse, Pirouette Reverse (the reversal before an omega turn), and Pirouette Forward (the subsequent resolution of the omega turn), as detailed in Supplementary Notes and Supplementary Table 1.

Wild-type animals loaded into a food-free, buffer-filled arena dispersed within minutes (Supplementary Video 2). Reversal, pause, and pirouette frequencies were elevated for the first 15–20 min in the device (Supplementary Fig. 5), characteristic of the local search behavior seen on agar following food removal[18–20], or reflecting adaptation to the novel arena environment. Animals traversed the entire 22 × 20 mm^2 arena, displaying sustained forward locomotion interspersed with occasional pauses, reversals, and pirouettes (Fig. 2b,c), and were insensitive to steady fluid flow (Supplementary Fig. 6). These macroscale behavioral patterns resembled those observed on agar surfaces, with a few exceptions (Supplementary Notes and Supplementary Fig. 7). After excluding behavior near the physical barriers, the remaining 81 ± 2% of data points were condensed into instantaneous behavioral state and speed vectors for each animal (Fig. 2d), and analyzed temporally or spatially depending on the stimulus pattern.

Behavioral responses to temporal odor patterns

We first examined odor-evoked behavioral dynamics by subjecting wild-type young adults to a series of attractive odor pulses (0.92 μM isoamyl alcohol, IAA) interspersed with buffer (Fig. 3a and Supplementary Video 3). The AWC sensory neuron pair, which is activated by IAA removal and inhibited by its addition[5], directs chemotaxis by stimulating reversals and pirouettes when odor levels fall; these reorientations contribute to a biased random walk chemotaxis strategy on agar[17,21,22]. Consistent with this model, a stimulus-aligned ethogram of instantaneous behavioral state revealed a sharp increase in pauses, reverses, and pirouettes immediately following each odor-removal step, and suppression of these behaviors during each odor pulse (Fig. 3b,c). The peak omega turn rate of ~1.5 min^{-1} after odor removal (Fig. 3d) matched previous experiments[5]. No modulation of any parameter was apparent in control experiments switching between two buffer solutions or in a sensory mutant (Fig. 3e,f). Thus, behavioral responses in microfluidic arenas were elicited by odor and closely resembled those on agar surfaces.

We also observed new behavioral features. First, odor response adaptation was asymmetric: whereas pirouette state probability returned to baseline 90 s after odor removal, no adaptation was observed up to 3 min after odor addition (Fig. 3c,d) with only partial recovery after 10 min (data not shown). Second, behavioral states had unique temporal properties. For example, pauses and reversals that were not followed by a pirouette rose and peaked more rapidly than reversals within a pirouette (Fig. 3e). Behavioral changes were apparent within 0.5 s of odor removal, underscoring the need to switch stimuli rapidly to fully capture behavioral dynamics.

Each odor-buffer switch occurred with highly reproducible dynamics (Fig. 3e and Supplementary Fig. 2), yet behavioral responses varied considerably. We classified each response as Pirouette, Reverse, or Forward, according to the animal's dominant behavioral state following each odor removal (Fig. 3g). Wild-type responses were divided among these groups, with 44 ± 6% (s.e.m., n = 6 experiments) performing pirouettes, 28 ± 4% reversing, and 28 ± 5% maintaining forward motion (Fig. 3f). Following removal of a 1,000-fold stronger odor stimulus, the pirouette state probability increased to 80 ± 2%, yet 7 ± 2% of these pulses still failed to elicit a reversal or pirouette. Odor addition suppressed the spontaneous pirouette response rate from 14 ± 3% to 4.0 ± 0.3%. We found no evidence that individual animals differed substantially from the population mean in response probability, or that responses to earlier pulses differed from later pulses (Fig. 3h). We also found only minor effects of experimental parameters such as position in the device, worm orientation and speed, odor pulse duration, odor gradient, and experimental time (Supplementary Fig. 8). Thus, step responses appear to be inherently probabilistic and occur with odor-regulated frequencies that are consistent across populations and repeated stimulations of individuals.

Behavioral responses to spatial odor patterns

We next tested responses to sharp spatial changes in odor by exposing animals to parallel stripes of IAA under laminar flow (Fig. 4a and Supplementary Video 4). At each stripe edge, animals experienced a sharp odor gradient but no flowrate or mechanical discontinuity. Wild-type worms accumulated in the attractive odor streams for over 80 min (Fig. 4b,c), localized equally to wide (5 mm) and narrow (1.5 mm) odor stripes, and resided preferentially at local odor maxima (Fig. 4d).

To analyze how animals reacted to sudden changes in odor concentration, we spatially averaged speed, behavioral state probabilities, and turning rates for animals heading inward (entering) or outward (exiting) near stripe edges (Fig. 4e,f and Supplementary Fig. 9). Outward-heading wild-type animals responded strongly with decreased forward speed and sharp spikes in reversals, pirouettes, and curves that prevented odor exit, whereas inward-directed animals reacted only weakly.

A peak in residence at the stripe edge reflected pauses and slowing prior to making a turn, as well as horizontal locomotion along the odor-buffer edge, which we call "surfing". Surfing often ended in a smooth curve unaccompanied by reversals or pauses, and nearly all of these "surf" curves led toward the odor (94.4 ± 1.4% s.e.m., n = 6 experiments, 335/355 total events, Fig. 4g). This strong directional bias could not be explained by the animal's weaker

tendency to curve gradually in one direction (Supplementary Fig. 9b) and suggests deliberate steering toward odor.

We next subjected two mutants defective for IAA chemotaxis on agar to IAA stripes: *tax-4*, which encodes a cGMP-gated ion channel required for AWC sensory transduction, and *eat-4*, which encodes a vesicular glutamate transporter required for glutamatergic neurotransmission by AWC[5]. Neither *tax-4* nor *eat-4* mutants accumulated in the odor stripes (Fig. 4e), and chemotaxis indices reflecting enrichment in odor were close to zero (Fig. 4h), as in agar assays. However, while *tax-4* mutants were defective for all behaviors elicited at the odor-buffer edge, *eat-4* mutants showed wild-type slowing behavior on exiting the odor and resided more at the odor edges (Fig. 4e,f,h). Overall, 13 of 43 quantitative behavioral parameters were significantly affected by odor in *eat-4* mutants, whereas no parameter differed between *tax-4* mutants and no-odor controls (Supplementary Fig. 10). The residual function in *eat-4* suggests the use of additional glutamate transporters or other transmitters by AWC, and indeed AWC also signals through neuropeptides[23]. Most (56–61%) behavioral parameters in each mutant were rescued by expression of the respective cDNA under the AWC promoter *odr-3* (Fig. 4e,f).

Analysis of individual odor-edge encounters

To analyze response variability in the stripe assay, we constructed “edge-triggered” ethograms by aligning behavioral rasters within a –30 s to +15 s time window relative to each odor edge crossing or turn initiated at the edge (Fig. 5a,b). We grouped edge encounters by approach (inward, horizontal, or outward), by response type (forward, curve, or pirouette), and by outcome, with “correct” turns preventing odor exit (Fig. 5c). The wild-type edge encounter rate rose over time proportional to speed (Fig. 5d), but the type and correctness of edge responses remained roughly stable for 80 mins before the onset of odor adaptation (Fig. 5e); subsequent analyses were performed within this time period.

We analyzed 2,208 outward edge responses from 159 wild-type animals in six experiments (10.5 outward events animal^{-1} hr^{-1}) and observed five distinct responses upon odor exit. An animal could (1) continue forward without turning, (2) reverse briefly, but then continue forward, (3) initiate a curve, (4) perform a reversal followed by a curve, or (5) perform a pirouette (Fig. 5f,g and Supplementary Video 5). Curve or pirouette behaviors (categories 3–5) could be either correct or incorrect, and showed similar average speed, position, and behavioral state trajectories with or without odor (Supplementary Fig. 11). Animals that did not turn or reverse (category 1) slowed briefly upon exiting odor but not buffer stripes, suggesting that they detected the odor edge but chose not to reorient themselves; this pure slowing response had not been described previously (Fig. 5h).

Outward odor edge responses were variable, like responses in the pulse assay: for every five edge encounters, the animal turned correctly three times (58 ± 6%), continued forward without turning once (23 ± 4% of encounters), and turned incorrectly once (20 ± 3%) (Fig. 5i). By contrast, no-odor controls and *tax-4* sensory mutants mostly continued forward across the stripe edge (54 ± 2% and 67 ± 1%) and turned back into the stripe infrequently by chance (15 ± 3% and 9 ± 1%, respectively). We asked whether any feature of wild-type behavioral history could predict response outcome. All response categories showed similar

speed and behavioral state probabilities until 15 s prior to the response (Supplementary Fig. 11). Within this period, the presence of a short reversal nearly tripled the likelihood of a subsequent correct turn (Supplementary Fig. 11f), perhaps by allowing repeated sampling of the stimulus or increasing the time available for decision-making.

Odor gradients

To examine the role of gradient steepness, we next quantified wild-type behavioral responses to a nearly linear odor ramp (0.15 ± 0.05 s.d. μM mm^{-1}) over 30 times shallower than the gradient at an odor stripe edge (Fig. 6a). Animals quickly moved up the gradient but did not remain at the concentration peak (Fig. 6b,c). Instead, they cycled up and down the gradient for 2 h, such that overall residence at a particular location in the arena correlated approximately with odor concentration (Fig. 6d).

All classes of turns showed directional bias in the shallow gradient, but significantly less than was observed in the steep gradients of a stripe assay. Pirouette turns were 2.5-fold more frequent in animals traveling down the shallow gradient than up the gradient ($P < 0.001$ vs. no-odor control), and surf curves were directed 80% more often up than down the gradient ($P = 0.06$); by contrast, pirouettes and surf curves showed 7.5-fold and >10-fold directional bias at odor stripe edges, respectively (Fig. 6e-g). We observed no directional difference in speed in the shallow odor gradient ($P > 0.3$), in contrast to sharp gradients (Fig. 6h), suggesting that orthotaxis plays little role in chemotaxis to shallow gradients.

DISCUSSION

These microfluidic assays confirm existing models for *C. elegans* chemotaxis and provide new quantitative and statistical insights into stimulus-evoked behaviors. We observed klinokinesis (biased pirouette probability) and klinotaxis (curving turns directed toward the odor), as previously shown[17,22], and orthotaxis (biased forward speed) in sharp gradients. We identified three new locomotory behaviors: a coupled short reversal-curve, a “surf” curve, and a pure slowing response. The short reversal-curve motor pattern results in a smaller reorientation than the long reversal-omega turn of a classical pirouette, but is nonetheless as frequent as the pirouette at an odor edge and as likely to result in a correct response. The accuracy of “surf” curves that bend smoothly toward the odor without corrective reversals suggests that *C. elegans* can detect the direction of the odor gradient and bias its head movements accordingly. These curves, especially prominent at high-gradient stripe edges, were also biased up shallow gradients; both surf curves and the reversal-curve pair may contribute to the directed “weathervane” klinotaxis observed on agar plates[22]. Lastly, the pure slowing response upon odor removal, the weakest detectable behavior, can occur without other turns and reversals. Slowing, pauses, and short reversals may all enable the worm to gather additional information about the changing environment before executing a more substantial turn.

Each response type showed stereotyped motion with nearly-identical dynamics whether spontaneous or odor-evoked, suggesting that locomotory behaviors are primarily drawn from a pre-existing set of motor patterns. Any of these behaviors could follow a sudden odor change over time or space, and individual responses were unpredictable but occurred at

consistent, stimulus-dependent probabilities over repeated stimuli and across animals. The population-average behavior probabilities provide a comprehensive, quantitative phenotype sensitive to perturbations in neural circuitry: chemotaxis-deficient mutants were easily distinguished from wild type and each other. Moreover, the normal speed modulation in *eat-4* but not *tax-4* suggests that distinct behaviors triggered by odor stimuli differ in their reliance on glutamate as a neurotransmitter.

Microfluidic arenas offer substantial advantages in the control and versatility of stimulus patterns. Chemical gradients were quantifiable and repeatable; consequently, assay results were consistent across experiments, users, devices, and time (Supplementary Fig. 12d). Gradient strength was tunable over two orders of magnitude by fluid flowrate, an easily-accessible experimental variable (Supplementary Fig. 1), enabling the presentation of square-wave or sinusoidal chemical patterns within the same experiment. The measurement of responses to different stimulus patterns generally yielded complementary but unique data. For example, pulse assays were ideal for measuring behavioral dynamics and variability by subjecting all animals to the same odor pattern, whereas stripe and gradient assays allowed assessment of turn orientation and taxis strategy but provided each animal a unique (though measurable) olfactory experience determined by its own movements.

Various liquid-borne stimuli can be presented in these devices, whether attractive or repulsive, and singularly or simultaneously: aqueous solutions, dissolved odors and gases, bacterial food, and fluids of defined temperature (Supplementary Fig. 12). All stimulus modalities are presented in the same physical environment, a hybrid liquid/solid structured environment that may resemble the natural soil habitat of *C. elegans*[14]. Alternate behavioral assays remain advantageous for specific applications; for example, the microdroplet assay[6] can screen behavior of several worms and recover them individually after the assay, whereas worms are recovered from our microfluidic arenas as a mixed population.

Overall, we designed these devices for simplicity in fabrication (as single-layer, unbonded silicone casts) and in operation (stimuli could be switched using standard Luer valves, and disassembled devices could be cleaned for reuse). Second-generation devices increased experimental throughput without compromising behavioral data (Supplementary Fig. 12), testing up to four separate populations and four stimuli simultaneously. Arenas are also compatible with more complex, automated fluidic designs, toward the integration of behavioral measurements with high-throughput screening[24], optogenetic analysis[25], and calcium imaging[11] within a single platform. By increasing the reliability and detail of behavioral measurements, the control and variety of imposed sensory environments, and the throughput of experiments, these microfluidic arenas should accelerate the study of neural circuit functions and their underlying genetic and molecular bases.

METHODS

Strains and worm preparation

C. elegans were maintained under standard conditions and fed with OP50 bacteria[26]. Wild-type animals were Bristol strain (N2). Other strains used in this study include: FK103 *tax-4 (ks28)*, CX5 *eat-4 (ky5)*, CX7535 *tax-4 (ks28); kyEx936 [odr-3::tax-4::GFP]*, and CX9066

eat-4 (ky5); kyEx1779 [odr-3::eat-4::sl2::CFP]; both transgenes were injected at 50 ng μL^{-1}. To provide age-synchronized young adults for each experiment, we picked L4-stage worms onto agar plates 15–20 h earlier (or 20–24 h prior for *eat-4* mutants, which grew more slowly). Immediately prior to each experiment, we gently transferred ~25 worms onto a fresh, unseeded agar plate with a small amount of bacteria. After removing excess bacteria, we flooded the plate with ~5 mL S-basal buffer (100 mM NaCl, 50 mM potassium phosphate, pH 6.0) and drew animals into the loading tubing using a 1-mL syringe.

Device fabrication

We prepared monolayer microfluidic devices using soft lithography[27]. Briefly, we fabricated silicon mold masters using conventional photolithographic techniques to pattern a 70 μm layer of SU8 2050 photoresist (Microchem) on 4 inch wafers (Silicon Quest). Sample photomask designs are available in Supplementary Data 1 online. We then prepared plastic mold masters from each silicon master in a two-step process. First, we cast a PDMS mold "positive" from the silicon master, embedding a 2" × 3" glass slide within to increase the rigidity of the PDMS cast. Next, we poured liquid polyurethane (Smooth-Cast 310, Smooth-On) over the PDMS "positive" and allowed it to cure. This process could be repeated several times to create many durable, reusable, and monolithic "negative" molds with 3D features nearly identical to the original silicon mold[28]. At the final stage, we cast ~5 mm thick PDMS devices (Sylgard 184 A and B, 1:10 by weight; Dow Corning) and cored inlet and outlet holes with a 1-mm dermal punch (Accuderm). Unlike most microfluidic devices that are irreversibly bonded to glass, plastic, or PDMS by plasma activation, these devices were reversibly sealed. Sealing required three features: (1) clean, flat device surfaces, (2) a hydrophobic-treated glass substrate, and (3) a glass upper support slide to allow the application of pressure via miniature binder clips. We exposed glass substrates to (tridecafluoro-1,1,2,2-tetrahydrooctyl)-1-trichlorosilane (United Chemical Technologies) vapor for 1 hr in vacuum to render them hydrophobic, and drilled inlet and outlet holes in the upper glass slide with a diamond-coated bit. We cleaned devices in 95% EtOH at least overnight to remove residual PDMS monomers and/or odor stimuli, rinsed them in water, and baked them for 30 min at 55 oC to evaporate any absorbed EtOH.

Stimulus flow control

We controlled the flow of buffers and stimulus odor streams with manual Luer valves or automated valves (Lee Corporation) actuated by computer with custom MATLAB scripts, a LabJack U3-HV digital controller, and a Valvebank 8 II actuator (Automate). We regulated flow velocities in the arena up to ~2 mm s^{-1} by gravity proportional to the height differential Δh between the stimulus and outflow reservoir surfaces (e.g., 1 mm s^{-1} velocity at Δh ~ 45 cm). The flowrate decreased by less than 1.3% hr^{-1} due to the reduction in fluid level at the stimulus reservoirs (–6 mm hr^{-1} total among all reservoirs at 1 mm s^{-1} and 3.3 mL hr^{-1}; we kept the outflow level constant via vacuum suction). We obtained faster flow by pressurizing the stimulus reservoirs with a regulated air tank (up to 8 mm s^{-1} at 35 kPa pressure), or with a syringe pump (Harvard Apparatus, up to 40 mm s^{-1}).

Experimental setup

We assembled the microfluidic arenas and degassed them in a vacuum dessicator for 5–10 min prior to loading a 5 wt% Pluronic F127 solution through the outlet port; these steps produced a bubble-free arena within minutes. The polymer solution acts as a surfactant, thereby filling the arena more completely than S-basal buffer alone, and also adsorbed to arena surfaces rendering them resistant to protein or bacterial fouling. Degassing the devices caused any remaining bubbles absorb rapidly into the PDMS. We connected tubing from the stimulus reservoirs to the arena and flushed the device with S-basal buffer. Next, we attached the loading tubing containing ~25 animals and gently injected them via syringe into the arena in ~1 min (Supplementary Video 2). Continuous buffer flow washed the loaded worms, removing any residual bacteria. Experiments began 30 min after removal from bacterial food, once local search behaviors subsided[19] (Supplementary Fig. 5) and typically after 15–20 mins of buffer flow in the device. Following each experiment, we flushed arenas with water and soaked them in ethanol for ≥24 h to remove any residual odor. Next, we rinsed devices in water, dried them in an air stream, and baked them at 55°C for 30 min. Following this cleaning procedure, buffer-buffer controls showed no response, and devices could be reused over 30 times.

Video acquisition and data analysis

We captured video at ~37 pixels mm^{-1} resolution and 2 frames per second with an Optronics MacroFire or PixelLink FireWire camera and a Zeiss microscope with 0.6x optics. We processed videos offline using custom MATLAB scripts to (1) segment each video frame, obtain morphological data for each animal, link centroids into worm tracks[29]; (2) classify the instantaneous behavioral state for each worm; and (3) analyze behavioral data with respect to temporal and/or spatial stimuli. Scripts are available online as Supplementary Software 1 (updates available at http://arenawormtracker.dyndns.org), and segmentation algorithms are described in greater detail in Supplementary Notes.

Supplementary Material

Refer to Web version on PubMed Central for supplementary material.

Acknowledgments

We thank S. Leibler for the use of his cleanroom facility, J. Larsch for control experiments and assistance with manual scoring of behavior, and members of the Bargmann laboratory for critical help, insight, and advice. This work was supported by the Howard Hughes Medical Institute and by the G. Harold and Leila Y. Mathers Foundation. C.I.B. is an Investigator of the Howard Hughes Medical Institute. D.R.A. holds a holds a Career Award at the Scientific Interface from the Burroughs Wellcome Fund.

References

1. Robinson DA. The use of control systems analysis in the neurophysiology of eye movements. Annu Rev Neurosci. 1981; 4:463–503. [PubMed: 7013640]
2. Branson K, Robie AA, Bender J, Perona P, Dickinson MH. High-throughput ethomics in large groups of Drosophila. Nat Methods. 2009; 6:451–7. [PubMed: 19412169]

3. Ward S. Chemotaxis by the nematode Caenorhabditis elegans: identification of attractants and analysis of the response by use of mutants. Proc Natl Acad Sci U S A. 1973; 70:817–21. [PubMed: 4351805]
4. Bargmann CI, Hartwieg E, Horvitz HR. Odorant-selective genes and neurons mediate olfaction in C. elegans. Cell. 1993; 74:515–27. [PubMed: 8348618]
5. Chalasani SH, et al. Dissecting a circuit for olfactory behaviour in Caenorhabditis elegans. Nature. 2007; 450:63–70. [PubMed: 17972877]
6. Luo L, Gabel CV, Ha HI, Zhang Y, Samuel AD. Olfactory behavior of swimming C. elegans analyzed by measuring motile responses to temporal variations of odorants. J Neurophysiol. 2008; 99:2617–25. [PubMed: 18367700]
7. Miller AC, Thiele TR, Faumont S, Moravec ML, Lockery SR. Step-response analysis of chemotaxis in Caenorhabditis elegans. J Neurosci. 2005; 25:3369–78. [PubMed: 15800192]
8. Takayama S, et al. Subcellular positioning of small molecules. Nature. 2001; 411:1016. [PubMed: 11429594]
9. Li Jeon N, et al. Neutrophil chemotaxis in linear and complex gradients of interleukin-8 formed in a microfabricated device. Nat Biotechnol. 2002; 20:826–30. [PubMed: 12091913]
10. Bennett MR, et al. Metabolic gene regulation in a dynamically changing environment. Nature. 2008; 454:1119–22. [PubMed: 18668041]
11. Chronis N. Worm chips: microtools for C. elegans biology. Lab Chip. 2010; 10:432–7. [PubMed: 20126682]
12. Ben-Yakar A, Chronis N, Lu H. Microfluidics for the analysis of behavior, nerve regeneration, and neural cell biology in C. elegans. Curr Opin Neurobiol. 2009; 19:561–7. [PubMed: 19896831]
13. Chronis N, Zimmer M, Bargmann CI. Microfluidics for in vivo imaging of neuronal and behavioral activity in Caenorhabditis elegans. Nat Methods. 2007; 4:727–31. [PubMed: 17704783]
14. Lockery SR, et al. Artificial dirt: microfluidic substrates for nematode neurobiology and behavior. J Neurophysiol. 2008; 99:3136–43. [PubMed: 18337372]
15. Park S, et al. Enhanced Caenorhabditis elegans locomotion in a structured microfluidic environment. PLoS One. 2008; 3:e2550. [PubMed: 18575618]
16. Croll NA. Behavioural analysis of nematode movement. Adv Parasitol. 1975; 13:71–122. [PubMed: 1169872]
17. Pierce-Shimomura JT, Morse TM, Lockery SR. The fundamental role of pirouettes in Caenorhabditis elegans chemotaxis. J Neurosci. 1999; 19:9557–69. [PubMed: 10531458]
18. Wakabayashi T, Kitagawa I, Shingai R. Neurons regulating the duration of forward locomotion in Caenorhabditis elegans. Neurosci Res. 2004; 50:103–11. [PubMed: 15288503]
19. Gray JM, Hill JJ, Bargmann CI. A circuit for navigation in Caenorhabditis elegans. Proc Natl Acad Sci U S A. 2005; 102:3184–3191. [PubMed: 15689400]
20. Hills T, Brockie PJ, Maricq AV. Dopamine and glutamate control area-restricted search behavior in Caenorhabditis elegans. J Neurosci. 2004; 24:1217–25. [PubMed: 14762140]
21. Tsunozaki M, Chalasani SH, Bargmann CI. A behavioral switch: cGMP and PKC signaling in olfactory neurons reverses odor preference in C. elegans. Neuron. 2008; 59:959–71. [PubMed: 18817734]
22. Iino Y, Yoshida K. Parallel use of two behavioral mechanisms for chemotaxis in Caenorhabditis elegans. J Neurosci. 2009; 29:5370–80. [PubMed: 19403805]
23. Chalasani SH, et al. Neuropeptide feedback modifies odor-evoked dynamics in Caenorhabditis elegans olfactory neurons. Nat Neurosci. 2010; 13:615–21. [PubMed: 20364145]
24. Chung K, Crane MM, Lu H. Automated on-chip rapid microscopy, phenotyping and sorting of C. elegans Nat Methods. 2008; 5:637–43. [PubMed: 18568029]
25. Stirman JN, Brauner M, Gottschalk A, Lu H. High-throughput study of synaptic transmission at the neuromuscular junction enabled by optogenetics and microfluidics. J Neurosci Methods. 2010; 191:90–3. [PubMed: 20538016]
26. Brenner S. The genetics of Caenorhabditis elegans. Genetics. 1974; 77:71–94. [PubMed: 4366476]
27. McDonald JC, et al. Fabrication of microfluidic systems in poly(dimethylsiloxane). Electrophoresis. 2000; 21:27–40. [PubMed: 10634468]

28. Desai SP, Freeman DM, Voldman J. Plastic masters-rigid templates for soft lithography. Lab Chip. 2009; 9:1631–7. [PubMed: 19458873]

29. Ramot D, Johnson BE, Berry TL, Carnell L, Goodman MB. The parallel worm tracker: a platform for measuring average speed and drug-induced paralysis in nematodes. PLoS One. 2008; 3:e2208. [PubMed: 18493300]

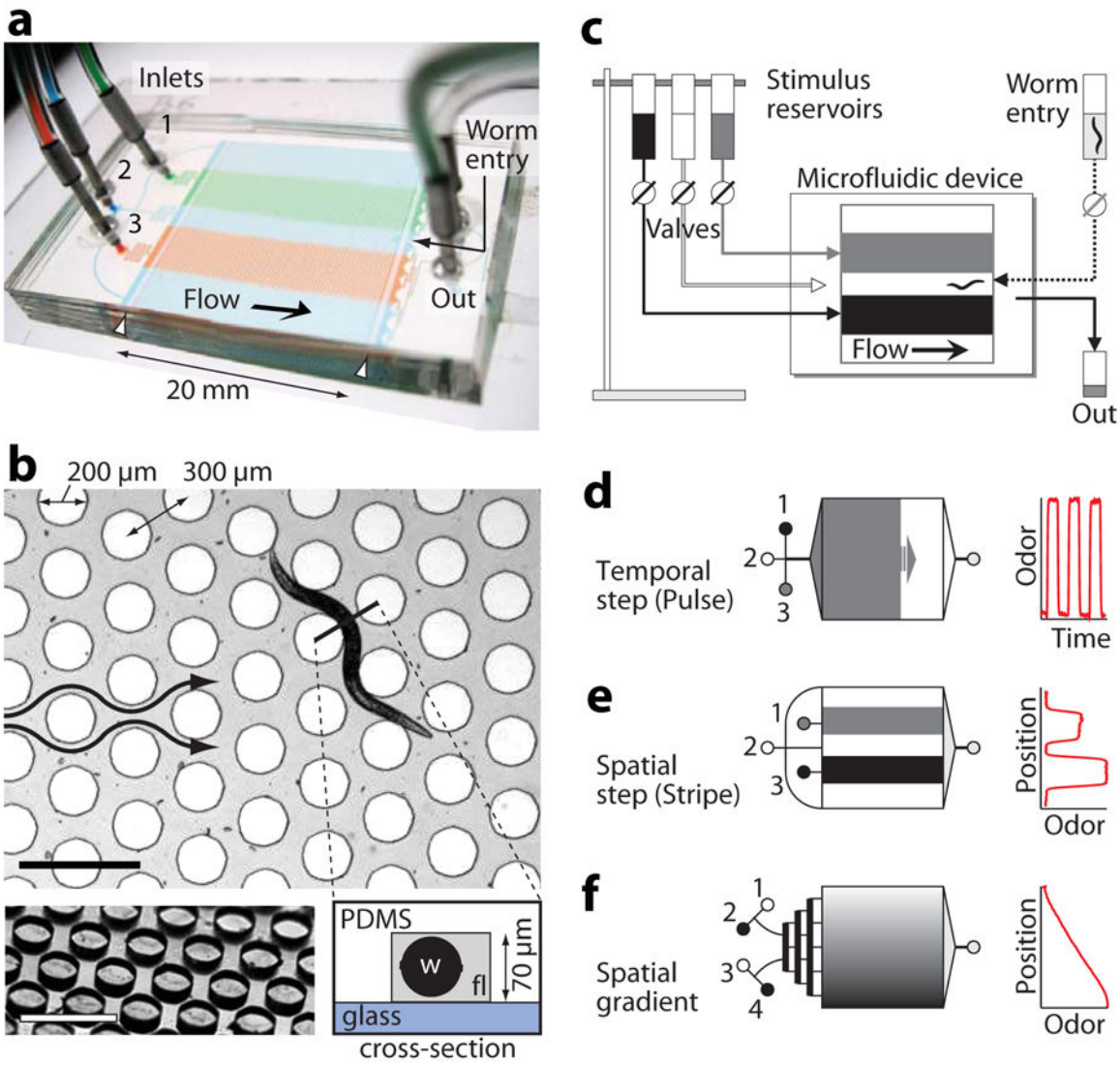

Figure 1.

Worm behavioral arena and stimulus patterns. (**a**) Photo of the microfluidic device, configured such that continuous flow of three streams (1–3) produces a stable pattern of dye stripes within the arena. Worm barriers prevent passage out of the arena (white arrowheads). (**b**) Top view showing arena geometry. A young adult worm crawls through fluid-filled channels (gray) between cylindrical microposts (white circles). Arrows indicate the direction of flow. Bottom left shows an oblique view of the micropost array before device assembly. Bottom right schematic shows a cross-section, indicating the glass bottom surface, PDMS top surface and posts, worm (w) and stimulus fluid (fl). Scale bars, 500 µm. (**c**) Stimuli flow by gravity from elevated reservoirs through external valves into the device. Worms are loaded with a syringe. (**d–f**) Upstream channels are tailored to each stimulus pattern: inlet channels converge to a distribution tree for stimulus pulses (**d**), remain separated for stimulus stripes (**e**), or pass though a mixing tree to create linear or sigmoidal concentration profiles (**f**). The graphs on the right show the corresponding odor patterns, estimated by measured dye concentration with respect to time or position in the device.

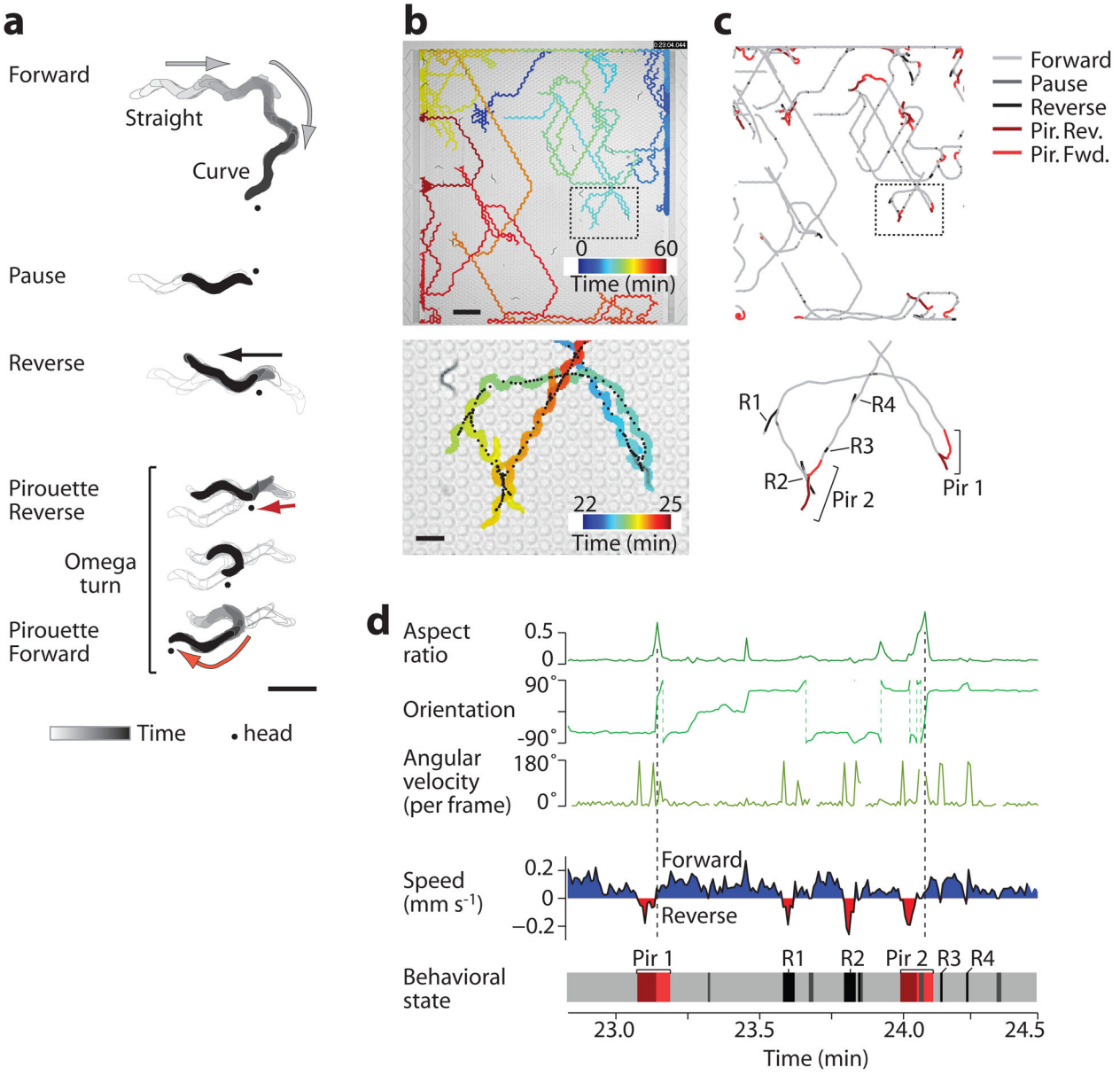

Figure 2.

Locomotory behavior in structured arenas. (**a**) Representative tracks from a single worm demonstrating the indicated behavioral states. Dot indicates the head of the worm. Arrows and shading show the direction of travel. (**b**) The path taken by one representative wild-type worm (of 24) over 1 hr shows navigation across the entire buffer-filled arena (above) and a magnified region (below). Color indicates time in the device. Black points indicate the animal centroid at 0.5 s intervals. (**c**) The centroid path for the animal in **b**, colored according to behavioral state. Swimming behavior at the upstream and downstream barriers was removed from analysis, and path breaks indicate temporary collisions with other animals. Specific reversal (R) and pirouette (Pir) behaviors are labeled in the magnified view below. (**d**) The graphs show the timecourse of morphological parameters (green plots, above) and speed (shaded plot, below) for the magnified worm path in **c**. The corresponding

behavioral state (bottom plot, colored as in **c**) was automatically determined from these parameters for each video frame (Supplementary Notes); for example, reversals are bounded by high angular velocity, and omega turns are identified by high aspect ratio and sharp reorientation (dashed lines). Labeled events correspond to the behavior trace in **c**. Scale bars, 500 μm (**a** and **b**, lower panel) and 2 mm (**b**, upper panel).

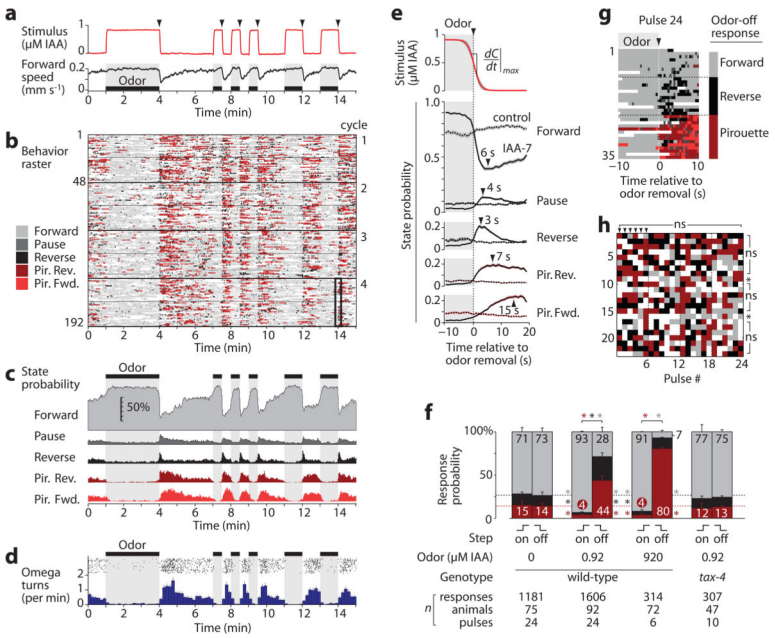

Figure 3.

Odor pulse assay. (**a**) Odor concentration estimated from dye absorbance during one cycle of IAA pulses (top), and corresponding instantaneous forward locomotion speed (bottom, *n* = 48 worms) are shown. (**b**) Ethogram showing the instantaneous behavioral state of animals subjected to the odor pattern in **a**. Each row represents one animal, and four 15-min cycles are shown stacked for a total of 192 rows. Speed traces and ethograms for each animal were aligned in time to the odor step it experienced. (**c**) Instantaneous behavioral state probability from **b**, excluding collisions and animals near the barriers. (**d**) Initiation of individual omega turns from **b** (black points, top) and average omega turn rate per animal (below, mean ± s.d.). (**e**) Average stimulus (top graph) and behavioral dynamics (lower graphs) for repeated odor removals (shading indicates 95% confidence for odor and s.e.m. for state probability, *n* = 24 pulses). Peak response times (arrows) are indicated. The dotted lines show buffer-buffer control switches. (**f**) Average probability of response to odor addition and removal (mean ± s.e.m., *n* = 6–24 pulses). Numbers indicate percent probability. *, $P < 0.01$ vs. wild-type odor-free probability of forward (gray), reverse (black), or pirouette (red) responses. (**g**) Ethogram showing a ±10 s window around odor removal #24 (black box in **b**), sorted by the predominant behavioral state after odor removal. (**h**) Responses of 23 individual animals to 24 repeated odor removal steps, colored as in **g**. *, $P < 0.05$; ns, not significant vs. the population mean by the mass function of the trinomial distribution and the Benjamini–Hochberg–Yekutieli correction for false discovery rate.

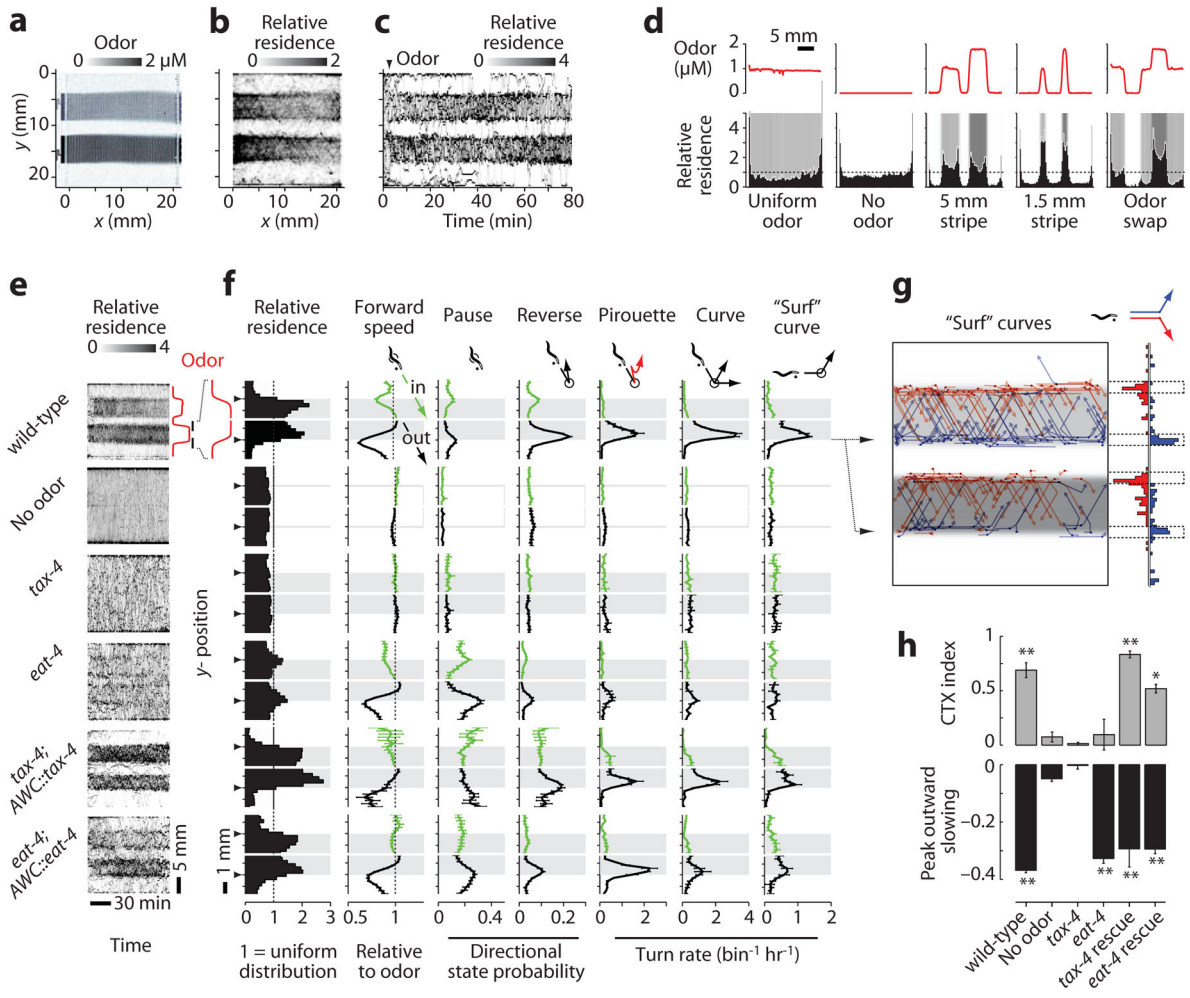

Figure 4.

Odor stripe assay. (**a**) The image shows the arena with two odor stripes containing 0.92 or 1.84 μM IAA and dye, surrounded by buffer. (**b**) Relative *x*-*y* residence of 24 worms over 80 min (a value of 1 represents a uniform distribution). (**c**) Timecourse of worm residence along the *y*-axis over time, with odor added at 3 min (arrowhead). (**d**) Histograms of residence relative to different spatial odor patterns (red plots above and shading below). (**e**) Heatmaps of wild-type, mutant, and rescued animal residence in odor or buffer stripes over time, as in **c**. (**f**) Spatially-averaged behavioral parameters within 1.8 mm surrounding each odor edge (arrowhead), as described in Supplementary Fig. 9. Shading indicates odor. Directional parameters are shown for animals traveling downward before the event, with the upper (green) and lower (black) plots representing inward and outward movement relative to odor, respectively. Dot indicates worm head, and event locations correspond to the animal centroid at event initiation (circle). Data are mean ± s.e.m., n = 2–10 experiments for turn rates, n = 8–24 odor edges for other parameters, averaged over 37–230 animals per condition. (**g**) Spatial plot and histogram of upward (blue) and downward (red) "surf" curves occurring within 0.5 mm of the odor edge (dotted lines), by 25 worms over 1 hr. (**h**) Top, mean chemotaxis (CTX) index from 20–80 min, defined as (animal density in odor – density out of odor)/(total density); below, peak outward forward speed relative to speed in odor.

Error bars as in **f**, with significance assessed by ANOVA and Bonferroni's correction for multiple comparisons. **, $P < 0.001$; * $P < 0.01$; ns, not significant compared with wild-type no-odor control.

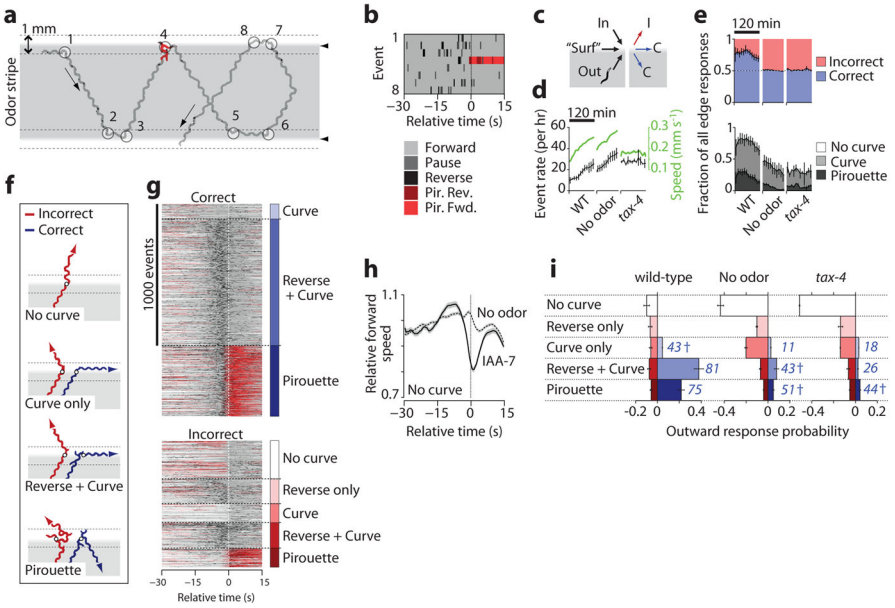

Figure 5.

Turning responses at sharp spatial odor gradients. (**a**) A wild-type worm track within a 0.92 μM IAA odor stripe (gray) shows turning events (circled) initiated within 0.5 mm of the odor edge (dotted lines) or odor edge crossings. (**b**) Ethogram shows –30 s to +15 s relative to the eight numbered edge encounter events in **a**. (**c**) Events were grouped according to the direction of edge approach (inward, “surfing” (horizontal), or outward) and by the response outcome (correctly remaining in the odor (C), or incorrectly leaving the odor (I)). All eight events in **a**,**b** are correct. (**d**) Outward edge event rates (black) for wild-type experiments with odor (WT) or buffer stripes (No odor) and *tax-4* with odor over 120 min, and average forward speed (green). (**e**) Correctness (above) and type (below) of all edge-triggered responses over 120 min. (**f**) Representative wild-type worm paths shown for correct and incorrect outward responses. Shading indicates odor. (**g**) Behavior rasters for wild-type worms heading outward, grouped by correctness and response category, n = 2,208 responses from 159 worms over 80 min. (**h**) Relative forward speed for WT animals that did not pirouette, curve or reverse upon exit of odor or buffer stripes. (**i**) Probabilities of outward responses for worms exiting odor and buffer stripes, indicating the percent correct for each category in blue. Data are mean ± s.e.m., n = 2–10 experiments. † indicates no significant difference from random (50% correct), $P > 0.2$ via two-tailed t-test.

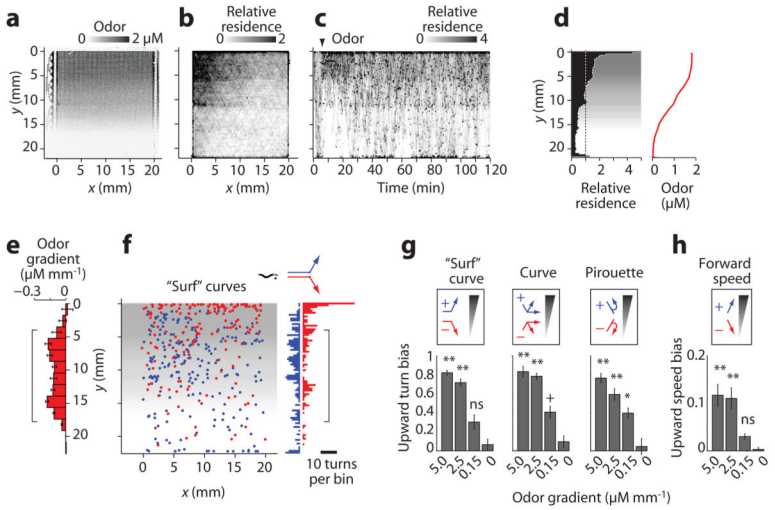

Figure 6.

Odor gradient assay. (**a**) Odor concentration gradient from 0–1.84 μM IAA in the arena, visualized with dye. (**b**) Relative *x*-*y* residence of 25 worms tracked over 120 min in the gradient; (a value of 1 represents a uniform distribution). (**c**) Timecourse of worm residence in the odor gradient, established at 5 min (arrowhead). (**d**) Distribution of wild-type worms over 120 min (average of 5 experiments) subjected to a spatial odor gradient (red plot and gray shading). (**e**) Odor concentration gradient calculated from odor profile in **d** (mean ± s.d., *n* = 6 points per 1.67 mm wide *y*-bin). (**f**) Location in the arena of "surf" curves directed up (blue) or down (red) the odor gradient. Bracket marks the region of constant odor gradient analyzed for turning bias. (**g**) Relative prevalence of "surf" curves, other curves, and pirouettes directed up (+1, blue) or down (–1, red) odor gradients from 0–5 μM mm^{-1} IAA. Indices on the y axis are defined as (# events up–# events down)/(total events per *y*-bin) averaged over the gradient region (bracketed in **e**, **f**). Bars indicate mean ± s.e.m., *n* = 5–9 *y*-bins averaged over 2–10 experiments. **, p<0.001; *, p<0.01; ns, not significant compared with wild-type no-odor control. Data for sharp gradients (≥2.5 μM mm^{-1}) were obtained with stripe device (Fig. 4). (**h**) Upward bias of forward speed, defined as (speed up gradient–speed down gradient)/(mean speed per *y*-bin); statistics as in **g**.